applied optics

Multistage single clad 2 μm TDFA with a shared L-band pump source

Robert E. Tench,[1,*] Clement Romano,[1,2] and Jean-Marc Delavaux[1]

[1]Cybel LLC, 1195 Pennsylvania Avenue, Bethlehem, Pennsylvania 18018, USA
[2]Institut Telecom/Paris Telecom Tech, 46 Rue Barrault, 75634 Paris, France
*Corresponding author: robert.tench@cybel-llc.com

Received 3 April 2018; revised 14 June 2018; accepted 15 June 2018; posted 15 June 2018 (Doc. ID 327569); published 12 July 2018

We report the experimental performance and simulation of a multiwatt two-stage TDFA using an L-band (1567 nm) shared pump source. We focus on the behavior of the amplifier for the parameters of output power P_{out}, gain G, noise figure NF, signal wavelength λ_s, and dynamic range. We measure the spectral performance of the TDFA for three specific wavelengths ($\lambda_s = 1909$, 1952, and 2004 nm) chosen to cover the low-, mid-, and upper-wavelength operating regions of the wideband amplifier. We also compare the performance of the two-stage shared pump TDFA with a representative one-stage shared pump amplifier. A comparison of experimental results with simulation is presented.

OCIS codes: (060.2310) Fiber optics; (060.2320) Fiber optics amplifiers and oscillators; (060.2390) Fiber optics, infrared; (060.2430) Fibers, single-mode.

https://doi.org/10.1364/AO.57.005948

1. INTRODUCTION

The broad bandwidth (BW) of single clad (SC) thulium-doped fiber amplifiers (TDFAs) has been demonstrated for different wavelength bands in applications ranging from telecommunications and lightwave systems [1–6] to spectral sensing, LIDAR, and short pulse generation [7–10]. Design optimization of amplifier architecture is critical for the practical realization of wideband, compact, and efficient TDFAs for these applications. Recently, we have reported results showing that SC-TDFAs can provide a combination of large gain (G) and high output power (P_{out}) over extended BWs [11–14]. In this work, we investigate the optimization of tandem SC amplifier topologies for wideband TDFAs. In particular, we focus on the simulation and experimental performance of a tandem (two-stage) SC-TDFA using an L-band (1567 nm) shared fiber laser pump source. We highlight the amplifier performance in the key areas of high P_{out}(>2 W), high G(>60 dB), low small signal noise figure (NF, <4 dB), and large dynamic range (>35 dB). We also evaluate the wavelength behavior of the SC-TDFA by measuring its performance at three specific wavelengths (1909, 1952, and 2004 nm), which are chosen to cover the low-, mid-, and upper-wavelength operating regions of the amplifier spectral response. We then contrast the performance of our tandem amplifier with that of a recent single-stage SC-TDFA. In comparing the topologies, we illustrate and discuss the tradeoffs for optimizing the TDFA configuration in a specific operating band.

The paper is organized as follows: Section 2 presents our experimental setup, a two-stage TDFA with a fixed pump coupling ratio between co-pumping and counter-pumping in the active fibers. Section 3 covers the dependence of experimental amplifier performance on signal input power (P_s), total P_p, and signal wavelength (λ_s). Section 4 compares measurement and simulation of the TDFA performance. Section 5 contrasts our simple TDFA design with performance of a one-stage shared pump design in Ref. [14]. Finally, Section 6 discusses design parameter tradeoffs for different TDFA architectures and applications.

2. EXPERIMENTAL SETUP FOR THE SHARED PUMP AMPLIFIER

The optical design of our two-stage single pump TDFA is shown in Fig. 1. A single frequency 2 μm input source (Eblana Photonics) is coupled through isolator I1 and wavelength division multiplexer WDM1 into the active fiber F1. Pump light from a multiwatt fiber laser P1 at 1567 nm is split by coupler C1 with a coupling ratio of 30%/70%. The two pump signals co-pump fiber F1 (30%) and counter-pump fiber F2 (70%), respectively. The signal output is coupled through I2 into F2, and the signal output of F2 then passes to the output through WDM2 and I3. I1–I3 ensure unidirectional operation and suppress backward ASE. F1 is 4.3 m, and F2 is 2.0 m of IXBlue Tm-doped SC silica fiber (IXF-TDF-4-125-v1). For the data reported in the experimental plots of Section 3, input

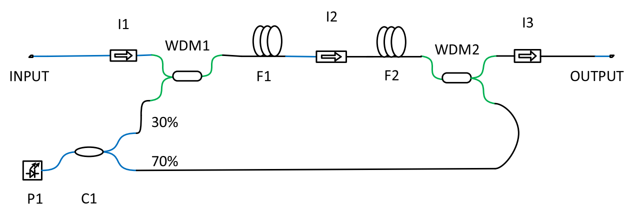

Fig. 1. Optical design of two-stage single-pump TDFA with a shared pump arrangement.

and output signal powers, and co-pump and counter-P_p, are, respectively, referenced to the inputs and outputs of F1 and F2 (internal G, power, and NF measurements.) Both internal and external performances of the amplifier are reported in the comparisons of Section 4. Optical power and optical spectra were measured with a Yokogawa AQ6375B optical spectrum analyzer (OSA).

3. EXPERIMENTAL AMPLIFIER PERFORMANCE (INTERNAL)

The first plot of experimental amplifier performance is in Fig. 2, which shows the variation in internal P_{out} as a function of total internal P_p for various levels of internal P_s at a λ_s of 1952 nm. For the maximum P_s of 1.6 dBm, $P_{\text{out}} = 1.82$ W at a total P_p of 3.61 W. The slope efficiency η for this input power, defined as $\eta = \Delta P_{\text{out}}/\Delta P_p$, is 54.2%. This slope efficiency is for the total amplifier, that is, for the total performance of Stage 1 and Stage 2. The optical-optical power conversion efficiency at this point is 1.82 W/3.61 W = 50.4%. The difference between slope efficiency η and optical-optical power conversion efficiency is caused by the zero crossing or threshold of the P_{out} curve, which crosses the P_{out} axis at a P_p of ≈0.28 W. Because of this threshold, the slope efficiency η can be significantly greater than the optical-optical power conversion efficiency.

Figure 3 plots the evolution of internal G as a function of P_p for various levels of P_s at 1952 nm. The G is defined in the following way:

$$G(\lambda_s) = P_{\text{out}}(\lambda_s)/P_s(\lambda_s). \tag{1}$$

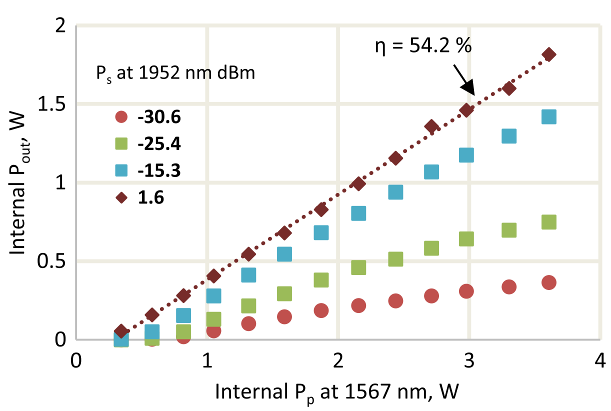

Fig. 2. P_{out} versus P_p for the parameter of P_s at 1952 nm. Points, data. Dashed line, linear fit to data.

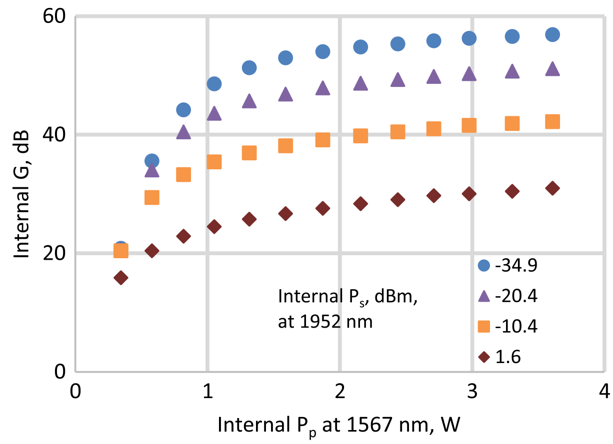

Fig. 3. G versus P_p for the parameter of P_s, at 1952 nm.

Note that G increases with increasing P_p as expected, and that the maximum G observed for $P_s = -35$ dBm is 56.9 dB. For $P_p = 3.61$ W, the 15 dB G saturation point occurs for $P_s \approx -7$ dBm. We note that $G = 50$ dB can be achieved for a P_p of only 1.2 W, illustrating the high G performance of the TDFA for low P_p.

Having established baselines for amplifier performance at $\lambda_s = 1952$ nm, we next investigate G and the NF as a function of λ_s.

For these studies, NF is defined by Eqs. (2)–(4), using the optical method of measurement [15,16]:

$$N_{\text{eq}}(\lambda) = P_{\text{ASE}}(\text{forward}, \lambda_s)/(2hc^2\Delta\lambda/\lambda_s^3)G(\lambda_s), \tag{2}$$

$$F(\lambda_s) = (1/G(\lambda_s)) + 2N_{\text{eq}}(\lambda_s), \tag{3}$$

$$\text{NF(dB)} = 10\ \log(F(\lambda_s)). \tag{4}$$

Here, P_{ASE} (forward, λ_s) is the forward amplified spontaneous emission (ASE) power from the output of the TDFA measured in the resolution BW $\Delta\lambda$ of the OSA, h is Planck's constant, and c is the speed of light in vacuum. $G(\lambda_s)$ is defined in Eq. (1). N_{eq} is the equivalent NF and F is the linear NF for the amplifier.

As an example of how to calculate the internal NF using Eqs. (1)–(4), we start with the two representative OSA output spectra from the TDFA for λ_s of 1952 and 2004 nm that are shown in Fig. 4. The internal input power for each of these spectra was −25.13 dBm at 2004 nm/ − 25.35 dBm at 1952 nm, and the resolution BW of the OSA was 1.0 nm. The measured optical signal to noise ratio (OSNR) of the input laser sources was >50 dB/1.0 nm. The calibration factor from the measured spectrum on the OSA to the actual internal P_{out} of the amplifier was measured to be 35.61 dB. Using the relationship $P_{\text{out}} = P_{\text{peak}} - P_{\text{ASE}}$ (see Fig. 4), the measured internal G of the amplifier was then determined to be 41.51 dB at 2004 nm and 54.10 dB at 1952 nm. From Fig. 4, we found the forward spontaneous P_{out} in a 1.0 nm BW to be −6.67 dBm ± 0.3 dBm (2.15×10^{-4} W) at 2004 nm and +6.84 dBm ± 0.3 dBm (4.83×10^{-3} W) at 1952 nm.

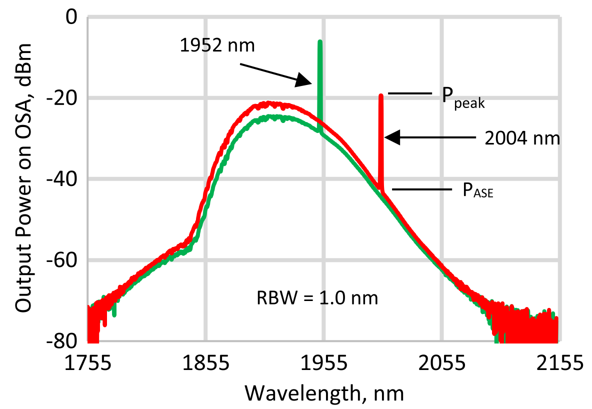

Fig. 4. Measured output spectra for the two-stage TDFA with internal $P_s \approx -25$ dBm and internal $P_p = 3.6$ W at 1567 nm.

These forward amplified spontaneous noise powers then yield the following NF values:

$$\text{internal NF at 1952 nm} = 3.65 \pm 0.3 \text{ dB},$$

$$\text{internal NF at 2004 nm} = 3.01 \pm 0.3 \text{ dB}.$$

Plots of these calculated internal NFs and the evolution of internal G and internal NF values for $P_p = 3.61$ W is plotted in Fig. 5 for the three experimental $\lambda_s = 1909$, 1952, and 2004 nm. We first note that G is maximum for 1909 nm and $P_s = -35$ dBm at 60.4 dB, decreasing to 56.9 dB at 1952 nm and 41.6 dB at 2004 nm. The 15 dB compression points are −13.5 dBm for 1909 nm, −12 dBm for 1952 nm, and $\approx +6$ dBm for 2004 nm. We also observe that small signal NF values are between 3 and 4 dB for all λ_s, rising to 4–5.8 dB for $P_s \approx 2$ dBm. The dynamic range of the amplifier is therefore 38 dB for the criterion of NF <5.8 dB. The internal NF over the total dynamic range is within 3 dB of the expected quantum limit of ≈3 dB for a quasi-two-level system, where the pump wavelength of 1567 nm is far from the λ_s of 1909–2004 nm. In such a system, the G at the pump wavelength is very small compared to Gs at the λ_s, resulting in an inversion that approaches the theoretical maximum.

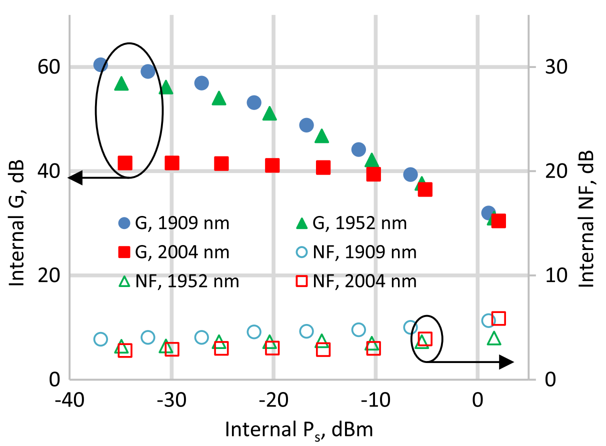

Fig. 5. Internal G and internal NF versus P_s for $P_p = 3.61$ W, at 1909, 1952, and 2004 nm.

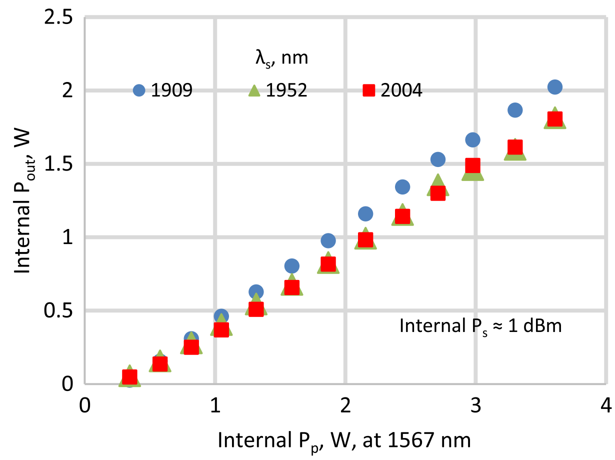

Fig. 6. Internal P_{out} versus internal P_p with the parameter of λ_s, for an Internal $P_s \approx 1$ dBm.

A graph of internal P_{out} versus P_p for the three λ_s studied is shown in Fig. 6 for $P_s \approx 1$ dBm. The maximum optical-optical conversion efficiencies are 56.2% for 1909 nm, 50.4% for 1952 nm, and 50.2% for 2004 nm. This plot illustrates a key behavior of the two-stage TDFA: variations in saturated P_{out} for the amplifier as a function of λ_s are relatively small, and high internal P_{out} of 1.8–2 W can be achieved over the ≈1.0 nm range of measured λ_s (for $P_s \approx 1$ dBm.)

A plot of slope efficiency η versus internal P_s for the three λ_s studied is given in Fig. 7. Maximum slope efficiencies are 62.3% for 1909 nm, 54.2% for 1952 nm, and 55.0% for 2004 nm. The evolution of the slope efficiency curves is quite different for 1909 and 1952 nm compared to 2004 nm. We observe that operation at the long wavelength of 2004 nm requires high input power to obtain high power conversion efficiency. This behavior is attributed to the variation in the amplifier saturation power as a function of λ_s [14] and will be studied further in a future publication.

Nonlinear effects, such as stimulated Brillouin scattering (SBS) or stimulated Raman scattering, were not observed in any of our measurements on the two-stage TDFA. This

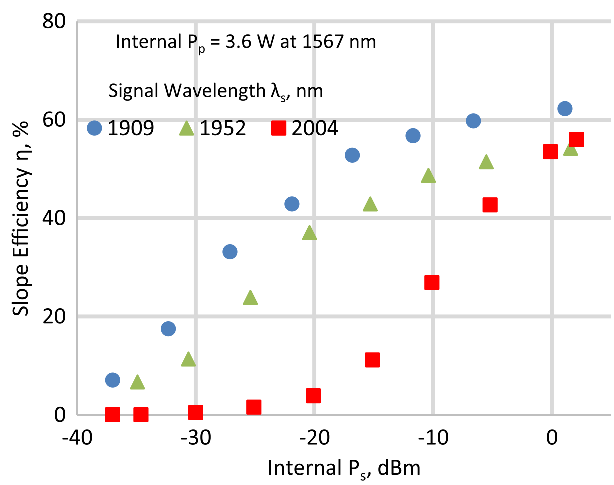

Fig. 7. Slope efficiency η versus internal P_s, with λ_s as the parameter.

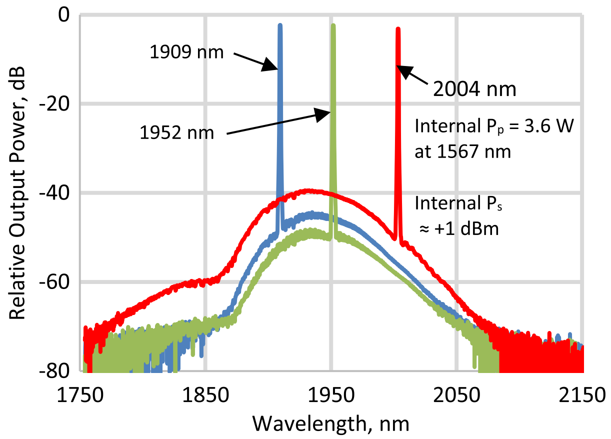

Fig. 8. Saturated output spectra for the tandem TDFA for three λ_s.

behavior is consistent with calculations of nonlinear thresholds for the Tm-doped fiber under investigation [17].

The experimental saturated output spectra for three λ_s of 1909, 1952, and 2004 nm are shown in Fig. 8. Here, the internal P_{out} is approximately 2 W, and the internal $P_p = 3.6$ W at 1567 nm for each of the three curves. The internal $P_s \approx +1$ dBm. The evolution of the ASE background as a function of λ_s is quite interesting. As illustrated in Fig. 8, the lowest ASE background occurs for $\lambda_s = 1952$ nm. The ASE increases slightly for $\lambda_s = 1909$ nm and, then, increases significantly for $\lambda_s = 2004$ nm. As with the behavior shown in Fig. 8, this ASE variation is attributed to the change in amplifier saturation power as a function of wavelength. Taking the estimated value of the amplifier BW from the points at which the ASE background is 15 dB down from the ASE peak, we can calculate BW = 139 nm for 1909 nm, 154 nm for 1952 nm, and 149 nm for 2004 nm. The average BW obtained from these values yields an estimated TDFA BW of 147 nm.

Key internal experimental parameters for the two-stage TDFA are summarized in Table 1 below. The largest observed difference is in the values of small signal G as a function of λ_s with a greatly decreased G for 2004 nm in comparison with 1909 and 1952 nm. All of the other parameters measured are similar, as a function of wavelength.

4. COMPARISON OF EXPERIMENT AND SIMULATION (INTERNAL AND EXTERNAL PERFORMANCE)

Next, we compare the experimental performance of the tandem SC-TDFA with steady state simulations of amplifier behavior.

Table 1. Summary Experimental Parameters for the Two-Stage TDFA in Fig. 1[a]

Experimental Parameter	1909 nm	1952 nm	2004 nm
Internal small signal G (dB)	60.4	56.9	41.6
Internal saturated P_{out}, (W)	2.02	1.81	1.82
Internal small signal NF (dB)	3.9	3.65	3.0
BW (nm)	139	154	149
Dynamic Range (dB)	38	38	38

[a]All of the values quoted are internal to the amplifier.

The theory, methods, and physical parameters underpinning the simulations are presented in detail in Refs. [11–14, 18–20]. In particular, Ref. [20] gives detailed plots of the absorption and G spectra for the IX Blue fiber used in the two-stage TDFA. Reference [20] also presents a comprehensive table of the physical parameters employed in the simulations, as well as detailed descriptions of the techniques used to measure level lifetimes, G spectra, and absorption spectra. The theory behind the simulations is described in Refs. [11–14].

Our first comparison of the experiment and simulation is shown in Fig. 9, which plots data for internal G and internal NF as a function of P_s for $P_p = 3.61$ W. Here, we find that the simulated values of G for 1952 nm vary from the experimental data by less than 1 dB. For 1909 nm, the simulation predicts values of small signal G that are about 3 dB larger than the experiment, and, for 2004 nm, the simulated values of small signal G are about 3 dB smaller than the experiment. The origin of these differences as a function of wavelength is under investigation. Even though some differences are observed, the general trends of the G simulations follow the experimental data closely.

The simulated internal NFs agree with the experimental data to within 2 dB for $\lambda_s = 1909$ nm and to within 1 dB for 1952 and 2004 nm. Again, the general trends of the simulations of NF follow the experimental values closely.

We now move from internal performance to external performance of the amplifier, using the signal and pump coupling loss values given in Table 2. Here, the input signal coupling is the loss from the input connector to the input of F1, the interstage signal coupling is the loss from the output of F1 to the input of F2, and the output signal coupling is the loss from the output of F2 to the output connector. The input pump coupling is the loss from the 1567 nm fiber pump laser to the input of F1, and the output pump coupling is the loss from the 1567 nm pump laser to the output of F2. These loss values are typical for the current generation of 2 μm optical components and can be expected to improve in the future.

Figure 10 plots the same information as shown in Fig. 8 for the external performance of the TDFA. Note that the fiber-to-fiber signal G is now reduced by the input signal coupling

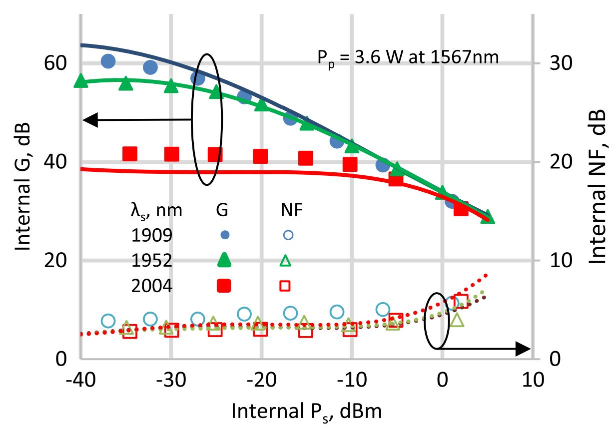

Fig. 9. Internal G and NF versus internal P_s with λ_s as the parameter. Points, data. Lines, simulations.

Table 2. Signal and Pump Coupling Losses for the Two-Stage TDFA in Fig. 1

Experimental Parameter	Loss Value (dB)
Input signal coupling	2.10
Interstage signal coupling	1.20
Output signal coupling	2.18
Input pump coupling (1567 nm fiber laser to F1)	5.96
Output pump coupling (1567 nm fiber laser to F2)	2.50

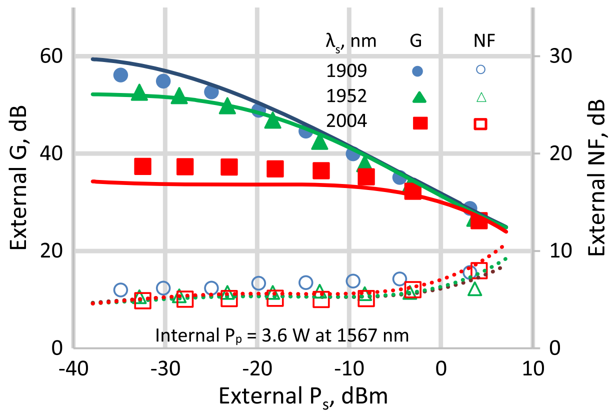

Fig. 10. External G and NF versus external P_s with λ_s as the parameter. Points, data. Lines, simulations.

and output signal coupling losses that equal 4.28 dB, and the NF and input power are now increased by the input coupling loss that equal 2.10 dB.

We next move to a comparison in Fig. 11 of internal P_{out} as a function of P_p for the three λ_s. In this graph, $P_s \approx 1$ dBm. For this case, the simulations predict slightly larger P_{out} than the experiments for all three wavelengths studied. For 1909 nm, the simulation predicts values 1.0 dB larger than the experiment; for 1952 nm, the difference is 0.8 dB; and, for 2004 nm, it is 0.4 dB. Similar differences have been observed in previous experimental and theoretical reports [12–14]. While the differences are measurable, we note that the simulations still yield saturated P_{out} values within 1.0 dB of the data for all wavelengths studied. This relatively good agreement

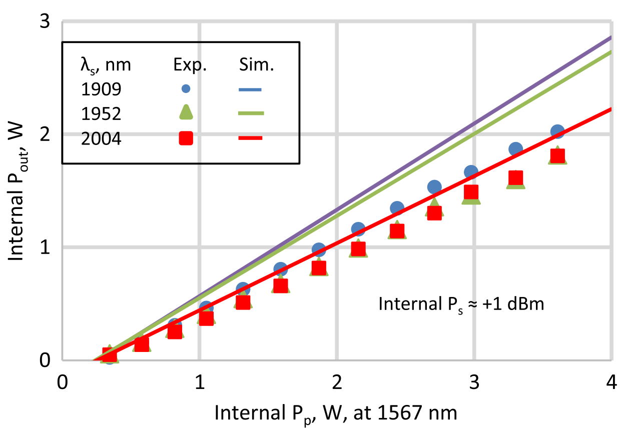

Fig. 11. Internal P_{out} versus internal P_p with λ_s as the parameter.

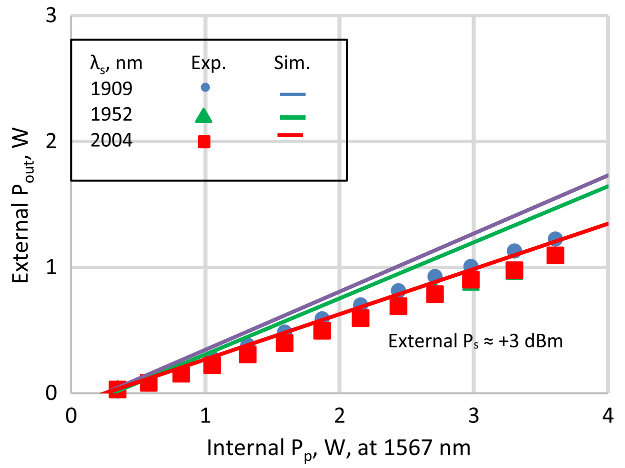

Fig. 12. External P_{out} versus internal P_p with λ_s as the parameter.

indicates that our simulations are a powerful tool for designing multistage SC TDFAs.

Figure 12 shows the plot of external P_{out} versus P_p for the parameter of λ_s. From Table 2, we find that the P_{out} are decreased relative to Fig. 11 by 2.18 dB or a factor of 0.605. Figure 12 illustrates that the maximum external P_{out} from the two-stage TDFA is 1.23 W at $\lambda_s = 1909$ nm.

By simulating P_{out} as a function of internal P_s and P_p, we next derived curves showing the variations in η as a function of P_s for the three λ_s studied. Plots of η versus P_s are shown in Fig. 13. As with the G curves in Figs. 8 and 9, we see that the general trends of the data are predicted well by the simulations.

In this case, the theory predicts somewhat larger values of η, relative to the experiment, for 1909 and 1952 nm. Somewhat smaller values of η are predicted for 2004 nm. Maximum predicted slope efficiencies are in the range of 63%–76.5%, while maximum measured slope efficiencies fall within the range of 56%–62%. This level of agreement is consistent with the differences observed between theory and experiment in the saturated P_{out} values plotted in Fig. 9. We note that the linear scale on the vertical axis of Fig. 13 highlights the differences between the experimental and simulated values, which on a logarithmic scale differ from one another by approximately 0–3 dB.

Another comparison of experiment and theory is given in Fig. 14, where measured and simulated values of η are plotted as a function of λ_s for two representative values of internal P_s (+1 and −20 dBm). As in Fig. 13, the trend is for predicted values of η to be larger than the measured values. Also as in Fig. 13, the linear vertical scale highlights the differences between the experiment and simulation. Nevertheless, we find that the trend of the simulated values is roughly similar to experiment. From this plot, it is clear that the operating BW of the amplifier is quite sensitive to the input power level. Defining BW as in Ref. [14] at the points at which the theoretical curves cross a threshold of $\eta = 50\%$, for +1 dBm, the BW is found to be >1.0 nm, while for −20 dBm it is 70 nm. The significant difference in BW as a function of P_s must be considered when designing preamplifiers, which typically operate with $P_s \approx -15$ to −30 dBm.

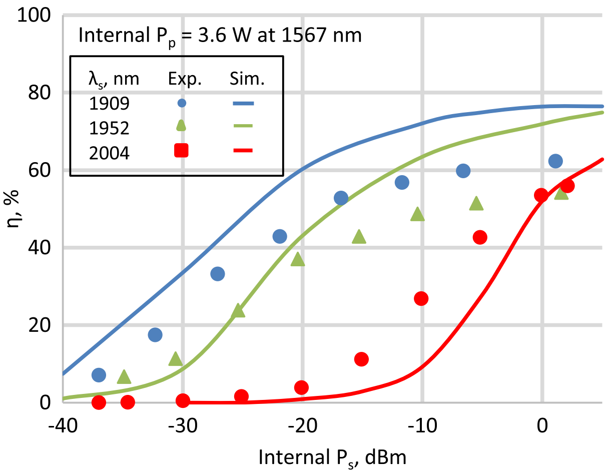

Fig. 13. η versus internal P_s with λ_s as the parameter.

5. COMPARISON OF TANDEM SHARED PUMP TDFA WITH SINGLE-STAGE SHARED PUMP AMPLIFIER PERFORMANCE

In Sections 3 and 4, we have shown that the shared pump tandem topology can deliver high performance that agrees reasonably well with simulation results. Here, we will compare the shared pump amplifier with a single-stage shared pump TDFA [14]. We observe here that the single-stage shared pump TDFA in Ref. [14] used a different Tm-doped fiber (OFS TmDF200) with a single-stage fiber length of 7.0 meters and a power split (pump coupling ratio) between forward and backward pumping of 50%/50%. Although there are differences between the constructions of the two amplifiers, we nevertheless find that a comparison of performance of the two amplifier architectures is valid and useful for the following reasons:

(1) The overall P_{out} and G behaviors of OFS TmDF200 Tm-doped fiber and IX Blue IXF-TDF-4-125-v1 Tm-doped fiber have been demonstrated to be roughly equivalent in spite of some small differences in power conversion efficiency and spectral characteristics. The similarities and relatively small differences between fiber performance are discussed in depth in Refs [12,13,20].

(2) We observe that a comparison of different amplifier architectures with roughly similar fiber Tm-doped fiber types is important for determining the relative performance of different designs, using fibers from diverse manufacturers, for high performance TDFA modules.

(3) The experimental and theoretical results in Ref. [14] demonstrate that the G, P_{out}, and NF performance of the single-stage shared pump TDFA with a 50%/50% coupling ratio are similar to its performance with a 30%/70% coupling ratio. We therefore expect that the difference in the coupling ratios between the one- and two-stage shared pump TDFAs will not materially affect the comparison.

Table 3 gives a summary comparison of the one- and two-stage shared pump TDFAs (parameters given are for internal amplifier performance at $\lambda_s = 1952$ nm).

The table reveals that there are some significant differences in performance between the two TDFAs and some similarities.

Table 3. Comparison of the Performance of TDFAs with Different Configurations

			TDFA Configurations $\lambda_s = 1952$ nm	
Parameter	**Symbol**	**Units**	**1 Stage, Shared Pump**	**2 Stage, Shared Pump**
Pump power (1567 nm)	P_p	W	3.2	3.6
Saturated output power	P_{out}	W	1.9	1.8
Small signal noise figure	NF	dB	3.4	3.65
Signal dynamic range	P_{in}	dB	32	38
Small signal gain	G	dB	51	57
Slope efficiency (saturated)	η	%	66	54
Operating bandwidth	BW	nm	167 (sim.)	147(est.) >160 (sim.)

Comparing the maximum saturated P_{out}, we see that the one-stage shared pump TDFA achieves 1.9 W internal P_{out} for 3.2 W available pump, while the two-stage shared pump amplifier achieves 1.8 W internal P_{out} for 3.6 W of available pump. The optical-optical power conversion efficiencies are then 59.4% for the one-stage configuration and 50.0% for the two-stage configuration. A similar difference is apparent in the measured values of η, which are 66% for the one stage and 54% for the two stages. This difference in optical-optical power conversion efficiency and in η is caused first by the measured difference in saturated power conversion efficiency for the two fiber types [12,13,20] and second by the insertion loss of I2, which is present in the two-stage design but not in the one-stage amplifier.

While the presence of I2 decreases η for the two-stage TDFA, it nevertheless enhances the overall performance of this configuration, especially for the parameters of small signal G and dynamic range. Table 2 shows that the maximum small signal G achieved with the one-stage design is 51 dB, while 57 dB can be achieved with the two-stage configuration. We note that there is a similar increase in dynamic range from 32 dB for one stage to 37 dB for two stages. The presence of I2 is responsible for the enhanced performance of the two-stage design because it suppresses self-lasing effects, which appear for high values of P_p and low values of P_s in the one-stage TDFA and also suppresses backward ASE from the second stage that would otherwise be coupled into the output of the first stage. The enhanced values of G and dynamic range are very important for telecommunications applications, such as in line repeaters and optical preamplifiers.

The minimum internal NFs that are achieved with the two configurations are 3.4 and 3.65 dB for one and two stages, respectively. These values are near the expected quantum limit of ≈3 dB, illustrating the high level of performance of our amplifier designs. The difference between the two values is relatively small and is not expected to result in a significant difference in lightwave system budgets.

Table 3 shows that the operating BW of the one-stage amplifier is 167 nm (simulated), while for the two-stage amplifier it is 147 nm (estimated from the ASE background) and >1.0 nm (derived from the simulation in Fig. 11). We observe, therefore, that the BWs of the two configurations are approximately equal. Design techniques, such as adjusting the lengths L1 and L2 of the two Tm-doped fibers in Fig. 1, can be used to increase the operating BW of the two-stage amplifier [14].

6. DISCUSSION OF PARAMETER OPTIMIZATION FOR TDFA ARCHITECTURES

The data reported in Figs. 2–14 illustrate several salient points about the operation of the shared pump TDFA.

From our experimental and theoretical studies here, and from the research reported in Ref. [14], it is evident that input power levels, saturated P_{out} targets, NF specifications, small signal G specifications, and operating signal BWs all depend in an interrelated way on the amplifier architecture. Design of an optimized amplifier requires a careful balancing of all of these performance targets for the available P_p and the fiber lengths L1 and L2.

For G amplifiers, Fig. 3 shows that it is very important to consider the input signal power level when choosing an optimum amplifier design. For example, at the coupling ratio of 30/70% and $\lambda_s = 1952$ nm, the internal fiber G for −35 dBm input is highest at 57 dB for a P_p of 3.6 W. For −20 dBm input, the optimum G is 51 dB; for −10 dBm input, it is 42 dB; and for +1.6 dBm input, it is 31 dB. Clearly, the design specifications of the TDFA must be carefully considered when choosing an optimum P_s for a preamplifier designed to operate at low P_s.

Also for G amplifiers, the internal G and internal NF values plotted for a P_p of 3.6 W in Fig. 5 show that λ_s is quite important in establishing G specifications as a function of λ_s. The minimum internal small signal G of 42 dB is observed at $\lambda_s = 2004$ nm, which is approaching the long-wavelength boundary of the useful TDFA G spectrum. This value is almost 20 dB smaller than the maximum observed internal G of 60.4 dB at 1909 nm. While this variation must be taken into account, it should be noted that a G of 35 dB or larger is usually sufficient for successful operation of an optical preamplifier for receivers in lightwave transmission systems. The NF values shown in Fig. 5 vary only slightly with λ_s and P_s. These small variations are highly desirable in a TDFA design and demonstrate the high level of performance and robust nature of our two-stage shared pump amplifier.

For power amplifiers, the data in Fig. 2 show that high internal P_{out} well in excess of 1 W can be obtained at $\lambda_s = 1952$ nm for P_s as low as −15 dBm. For $P_s \approx 1$ dBm, internal P_{out} close or equal to 2 W are achieved for all three λ_s of 1909, 1952, and 2004 nm, as illustrated by the data in Fig. 5. The measured P_{out} scale linearly with P_p up to the maximum P_p used of 3.6 W. This demonstrates the high performance achieved with our two-stage design.

No SBS or other nonlinear effects were observed in our experiments. This means that we can improve the P_{out} of the amplifier simply by increasing the P_p up to the limit where nonlinear effects start to be observed. The threshold for SBS in our shared pump two-stage amplifier is currently under study and is initially estimated to be on the order of $P_{\mathrm{out}} \approx 12-15$ W [17].

Also for power amplifiers, variations in η as a function of P_s are illustrated in Fig. 13 for both experimental data and simulations. Here, we see that the saturation behavior of the amplifier is quite different near the high-wavelength boundary (2004 nm) of the Tm-doped fiber G spectrum, relative to performance at the center of the spectral band (1952 nm) and near the low-wavelength boundary (1909 nm). This variation with P_s must be considered carefully in the design of wide BW power amplifiers.

For generic or multipurpose amplifiers, such as in-line amplifiers, Fig. 8 shows quite interesting variations in the background ASE as a function of λ_s. As discussed in Section 3, we believe the variation in ASE levels is caused by variations in the saturation power of the amplifier with λ_s. This point is under study and will be considered more fully in a future publications. The ASE background must be carefully considered when designing in-line repeaters for concatenated lightwave systems in the 2 μm region.

To conclude, we have shown that active fiber lengths L1 = 4.4 m and L2 = 2 m of IXBlue IXF-TDF-4-125-v1 Tm-doped fiber, together with a pump coupling ratio of 30% co-pumping and 70% counter-pumping, provide balanced performance over a wide range of operating parameters for the two-stage shared pump TDFA configuration.

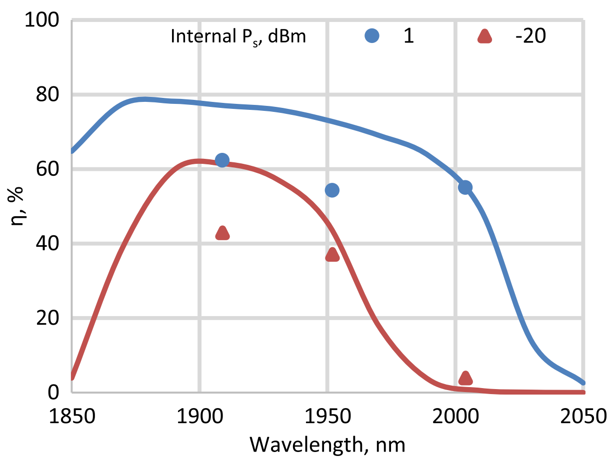

Fig. 14. Slope efficiency η as a function of λ_s. Points, data. Solid lines, simulations.

7. SUMMARY

We have reported the experimental and simulated performance of a tandem SC-TDFA with a shared in-band pump at 1567 nm. We measured and simulated the performance of the TDFA for parameters, such as λ_s band, saturated P_{out}, NF, small signal G, and dynamic range. Our measurements and simulations show that the simulated operating BW of the amplifier can be wider than 160 nm. We achieved internal saturated output powers of 2 W, internal small signal Gs as high as 60.4 dB, internal NFs as low as 3.0 dB, and a dynamic range of 38 dB for an internal NF of less than 5.6 dB. Comparison of the simulation and experiment yielded agreements of 0.4–1.0 dB in saturated P_{out} and 1–3 dB in small signal G over the experimental wavelength range studied of 1909–2004 nm. No Brillouin scattering or other nonlinear effects were observed in any of our measurements.

For our amplifier, the external G values were 4.28 dB smaller than the internal G; the external P_{out} were 2.13 dB smaller than the internal P_{out}; and the external NFs were 2.1 dB greater than the internal values. These differences are representative of the performance of current optical components and splices in the 2 μm wavelength band. We expect that the external performance of the amplifier will improve as the insertion losses of the components and splices are reduced in the future.

Our experiments and simulations show that the two-stage shared pump TDFA can largely match the performance of the single-stage shared pump amplifier reported in Ref. [14]. In addition, the two-stage amplifier has several advantages over the single-stage design.

First, the presence of an interstage isolator prevents self-lasing for both small input powers ($P_s \approx -30$ dBm) and for λ_s of 1909 and 2004 nm, which are approaching the upper and lower edges of the useful Tm G band. Self-lasing was observed in the single-stage shared pump amplifier for input powers lower than −20 dBm and P_p greater than about 1.6 W.

Second, the interstage isolator improves the dynamic range of the two-stage amplifier by 6 dB in comparison to the single-stage TDFA by preventing self-lasing and also by blocking backward ASE from the second stage.

Third, while the two-stage design is somewhat more complex than the one-stage configuration, it nevertheless yields better performance in the areas discussed above.

Finally, we observe that increasing the P_p slightly for the two-stage shared pump TDFA will compensate for the lower value of η in comparison to the one-stage design. We also note that the operating BW of the two-stage amplifier can be increased by adjusting the lengths L1 and L2 of the active Tm-doped fibers [14].

Taken together, the significant advantages we have demonstrated for the two-stage shared pump TDFA open the possibility for new and efficient 2 μm optical amplifiers for lightwave transmission systems as preamplifiers, wideband in-line amplifiers, and wideband power booster amplifiers.

Acknowledgment. We thank IX Blue Photonics for the single-clad Tm-doped fibers, and Eblana Photonics for the single-frequency discrete mode lasers in the 2000 nm band.

REFERENCES

1. Z. Li, A. M. Heidt, J. M. O. Daniel, Y. Jung, S. U. Alam, and D. J. Richardson, “Thulium-doped fiber amplifier for optical communications at 2 μm,” Opt. Express **21**, 9289–9297 (2013).
2. Z. Li, A. M. Heidt, N. Simakov, J. M. O. Daniel, S. U. Ulam, and D. J. Richardson, “Diode-pumped wideband thulium-doped fiber amplifiers for optical communications in the 1800–2050 nm window,” Opt. Express **21**, 26450–26455 (2013).
3. M. N. Petrovich, F. Poletti, J. P. Wooler, A. M. Heidt, N. K. Baddela, Z. Li, D. R. Gray, R. Slavík, F. Parmigiani, N. V. Wheeler, J. R. Hayes, E. Numkam, L. Grűner-Nielsen, B. Pálsdóttir, R. Phelan, B. Kelly, J. O’Carroll, M. Becker, N. MacSuibhne, J. Zhao, F. C. Garcia Gunning, A. D. Ellis, P. Petropoulos, S. U. Alam, and D. J. Richardson, “Demonstration of amplified data transmission at 2 μm in a low-loss wide bandwidth hollow core photonic bandgap fiber,” Opt. Express **21**, 28559–28569 (2013).
4. A. M. Heidt, Z. Li, and D. J. Richardson, “High power diode-seeded fiber amplifiers at 2 μm—from architectures to applications,” IEEE J. Sel. Top. Quantum Electron. **20**, 525–536 (2014).
5. Z. Li, Y. Jung, J. M. O. Daniel, N. Simakov, M. Tokurakawa, P. C. Shardlow, D. Jain, J. K. Sahu, A. M. Heidt, W. A. Clarkson, S. U. Alam, and D. J. Richardson, “Exploiting the short wavelength gain of silica-based thulium-doped fiber amplifiers,” Opt. Lett. **41**, 2197–2200 (2016).
6. Z. Li, “Thulium-doped fiber sources for novel applications,” Ph.D. thesis (Optoelectronics Research Center, University of Southampton, 2015).
7. D. Kracht, H. Sayink, S. Yilmaz, M. Wysmolek, K. Hausmann, M. Ottenhues, D. Wandt, A. Wienke, and J. Neumann, “Innovative laser sources operating around 2 μm,” Phys. Procedia **83**, 1184–1195 (2016).
8. H. Xia, G. Shentu, M. Shangguan, X. Xia, X. Jia, C. Wang, J. Zhang, J. S. Pelc, M. M. Fejer, Q. Zhang, X. Dou, and J.-W. Pan, “Long-range micro-pulse aerosol lidar at 1.5 μm with an upconversion single-photon detector,” Opt. Lett. **40**, 1579–1582 (2015).
9. F. Gibert, A. Dumas, J. Rothman, D. Edouart, C. Cenac, and J. Pellegrino, “Performances of a HGCDTE APD based direct detection lidar at 2 μm. Application to dial measurements,” EPJ Web Conf. **176**, 01001 (2018).
10. S. Ishii, A. Sato, M. Aoki, K. Akahane, S. Nagano, P. Baron, K. Mizutani, S. Ochiai, and M. Kubota, “Research and development for future space-based Doppler wind lidar,” in *Proceedings of 18th Coherent Laser Radar Conference*, Boulder, Colorado, June 2016, paper M-10.
11. C. Romano, R. E. Tench, Y. Jaouen, and G. Williams, “Simulation and design of a multistage 10 W thulium-doped double clad silica fiber amplifier at 2050 nm,” Proc. SPIE **10083**, 100830H (2017).
12. R. E. Tench, C. Romano, and J.-M. Delavaux, “Broadband 2 W output power tandem thulium-doped single clad fiber amplifier at 2 μm,” IEEE Photon. Technol. Lett. **30**, 503–506 (2018).
13. C. Romano, R. E. Tench, Y. Jaouen, and J.-M. Delavaux, “Characterization of the 3F4–3H6 transition in thulium-doped silica fibres and simulation of a 2 μm single clad amplifier,” in *European Conference on Optical Communication*, Gothenburg, Sweden, 2017, paper P1.SC1.2.
14. R. E. Tench, C. Romano, and J.-M. Delavaux, “Optimized design and performance of a shared pump single clad 2 μm TDFA,” Opt. Fiber Technol. **42**, 18–23 (2018).
15. E. Desurvire, *Erbium-Doped Fiber Amplifiers: Principles and Applications* (Wiley Interscience, 1994).
16. D. M. Baney, P. Gallion, and R. S. Tucker, “Theory and measurement techniques for the noise figure of optical amplifiers,” Opt. Fiber Technol. **6**, 122–154 (2000).
17. A. Sincore, N. Bodnar, J. Bradford, A. Abdulfattah, L. Shah, and M. C. Richardson, “SBS threshold dependence on pulse duration in a 2053 nm single-mode fiber amplifier,” J. Lightwave Technol. **35**, 4000–4003 (2017).
18. S. D. Jackson and T. A. King, “Theoretical modeling of Tm-doped silica fiber lasers,” J. Lightwave Technol. **17**, 948–956 (1999).
19. M. Gorjan, T. North, and M. Rochette, “Model of the amplified spontaneous emission generation in thulium-doped silica fibers,” J. Opt. Soc. Am. B **29**, 2886–2890 (2012).
20. C. Romano, R. E. Tench, and J.-M. Delavaux, “Simulation of 2 μm thulium-doped single clad silica fiber amplifiers by characterization of the $^3F_4$-$^3H^6$ transition,” Opt. Express (to be published).